Chinese Journal of Natural Medicines

Picroside II promotes HSC apoptosis and inhibits the cholestatic liver fibrosis in Mdr2$^{/}$ mice by polarizing M1 macrophages and balancing immune responses

Kexin JIA, Zhi MA, Yinhao ZHANG, Kaihong XIE, Jianan LI, Jianzhi WU, Jiaorong QU, Fanghong LI, Xiaojiaoyang LI

Citation: Kexin JIA, Zhi MA, Yinhao ZHANG, Kaihong XIE, Jianan LI, Jianzhi WU, Jiaorong QU, Fanghong LI, Xiaojiaoyang LI, Picroside II promotes HSC apoptosis and inhibits the cholestatic liver fibrosis in Mdr2$^{/}$ mice by polarizing M1 macrophages and balancing immune responses, Chinese Journal of Natural Medicines, 2024, 22(7), 582−598. doi: 10.1016/S1875−5364(24)60571−6.

View online: https://doi.org/10.1016/S1875−5364(24)60571−6

Available online at www.sciencedirect.com
ScienceDirect
Chinese Journal of Natural Medicines 2024, **22**(7): 582-598
doi: 10.1016/S1875-5364(24)60571-6
Chinese Journal of Natural Medicines

•Original article•

Picroside II promotes HSC apoptosis and inhibits the cholestatic liver fibrosis in Mdr2$^{-/-}$ mice by polarizing M1 macrophages and balancing immune responses

JIA Kexin[1Δ], MA Zhi[1Δ], ZHANG Yinhao[1], XIE Kaihong[1], LI Jianan[1], WU Jianzhi[1], QU Jiaorong[1], LI Fanghong[2], LI Xiaojiaoyang[1*]

[1] *School of Life Sciences, Beijing University of Chinese Medicine, Beijing 100029, China;*
[2] *School of Chinese Materia Medica, Beijing University of Chinese Medicine, Beijing 100029, China*

Available online 20 Jul., 2024

[ABSTRACT] Liver fibrosis is characterized by chronic inflammatory responses and progressive fibrous scar formation. Macrophages play a central role in the pathogenesis of hepatic fibrosis by reconstructing the immune microenvironment. Picroside II (PIC II), extracted from Picrorhizae Rhizoma, has demonstrated therapeutic potential for various liver damage. However, the mechanisms by which macrophage polarization initiates immune cascades and contributes to the development of liver fibrosis, and whether this process can be influenced by PIC II, remain unclear. In the current study, RNA sequencing and multiple molecular approaches were utilized to explore the underlying mechanisms of PIC II against liver fibrosis in multidrug-resistance protein 2 knockout (Mdr2$^{-/-}$) mice. Our findings indicate that PIC II activates M1-polarized macrophages to recruit natural killer cells (NK cells), potentially *via* the CXCL16-CXCR6 axis. Additionally, PIC II promotes the apoptosis of activated hepatic stellate cells (aHSCs) and enhances the cytotoxic effects of NK cells, while also reducing the formation of neutrophil extracellular traps (NETs). Notably, the anti-hepatic fibrosis effects associated with PIC II were largely reversed by macrophage depletion in Mdr2$^{-/-}$ mice. Collectively, our research suggests that PIC II is a potential candidate for halting the progression of liver fibrosis.

[KEY WORDS] Liver fibrosis; Picroside II; M1 macrophage; Hepatic stellate cell; Natural killer cell; Neutrophil
[CLC Number] R965 **[Document code]** A **[Article ID]** 2095-6975(2024)07-0582-17

Introduction

Hepatic fibrosis is a complex pathological process characterized by recurrent inflammation induced by various hepatic injuries, leading to fibrous scar formation due to the dysregulated overproduction and gradual accumulation of excessive extracellular matrix (ECM) [1]. If uncontrolled, this process can progress to severe liver diseases such as cirrhosis and hepatocellular carcinoma. Throughout this process, inflammatory reactions triggered by hepatocellular injury or necrosis of hepatic parenchymal or non-parenchymal cells are major risk factors for the initiation and development of liver fibrosis. The infiltration of inflammatory immune cells and their released chemotactic peptides interact, ultimately amplifying the activation of hepatic stellate cells (HSCs) [2]. To address the challenges in developing anti-fibrosis drugs, Ocaliva, an agonist of the nuclear receptor farnesoid X receptor (FXR), has emerged as a crucial regulator in hepatic fibrosis and has received Food and Drug Administration's (FDA) approval for the treatment of biliary fibrosis. However, its side effects, including pruritus, fatigue, abdominal pain, immunologic derangement, dizziness, and, in severe cases, acute liver failure, have limited its widespread use and application [3]. Therefore, there is an urgent need to explore the pathogenesis and identify specific targets for novel drugs to alleviate liver fibrosis.

The deficiency of multidrug resistance protein 2 (Mdr2), a crucial transport protein closely associated with bile secre-

[Received on] 11-Jan.-2024
[Research funding] This work was supported by the National Key Research and Development Program on Modernization of Traditional Chinese Medicine (No. 2022YFC3502100); the National Natural Science Foundation of China (No. 82274186); the National High-Level Talents Special Support Program; the Young Talents Promotion Project of China Association of Traditional Chinese Medicine (No. 2020-QNRC2-01); the Innovation Team and Talents Cultivation Program of National Administration of Traditional Chinese Medicine (No. ZYYCXTD-C-202006).
[*Corresponding author] E-mail: xiaojiaoyang.li@bucm.edu.cn
ΔThese authors contributed equally to this work.
These authors have no conflict of interest to declare.

tion, results in the accumulation of toxic bile acids and subsequent hepatocyte and cholangiocyte injuries, effectively mimicking the clinical pathological characteristics of primary sclerosing cholangitis (PSC) and other cholestatic liver fibrosis conditions [2, 4, 5]. The Mdr2 knockout ($Mdr2^{-/-}$) mouse is a well-established advanced fibrotic model widely used for investigating the pathogenesis of liver fibrosis and evaluating drug efficacy [6, 7]. Targeting inflammatory pathways or influencing immune cells has shown promise in recent anti-fibrotic therapies. Specifically, M1- and M2-like monocyte-derived macrophages are tightly associated with sclerosing cholangitis in $Mdr2^{-/-}$ through chemokines like the CCL2-CCR2/CCR5 axis and FXR-related pathways [8-10]. This highlights that abnormal changes in macrophages are not only features but also indispensable initial participants in hepatic fibrosis. Gevitha *et al.* focused on how the absence of interferon-gamma (IFN-γ)-mediated signaling influences the production of chemokines and immune cell recruitment, ultimately affecting liver fibrosis in the $Mdr2^{-/-}$ mouse model. They confirmed that increased levels of IFN-γ promote the expression of granzyme B (GZMB) from $CD8^+$ T and natural killer (NK) cells, which further results in the inhibition of activated hepatic stellate cells (aHSCs) and the alleviation of liver fibrosis [11]. Additionally, low doses of interleukin-2 (IL-2) were shown to inhibit hepatic $CD8^+$ lymphocyte proliferation, thereby reducing fibrosis in $Mdr2^{-/-}$ mice [12]. However, the potential mechanisms underlying the pathological transformation from hepatic inflammation to fibrosis and the complex crosstalk between multiple immune cells, particularly macrophages and NK cells, that lead to hepatic fibrosis in $Mdr2^{-/-}$ mice have not been fully elucidated.

Picroside II (PIC II), a prominent active component of Picrorhizae Rhizoma, has demonstrated therapeutic potential for ischemia/reperfusion injury, liver damage, and cancer metastasis through its anti-inflammatory, antioxidant, and anti-angiogenic properties [13, 14]. Recently, researchers have increasingly focused on the hepatoprotective and immunoregulatory functions of PIC II. In an *α*-naphthyliso thiocyanate-induced cholestasis mouse model, PIC II significantly activated FXR, thereby regulating the activities of bile acid efflux transporters and bile acid metabolizing enzymes in the liver [13]. Additionally, bile acids are known to influence the immune system by balancing the gut microbiome or acting as signaling molecules [15], suggesting that PIC II might directly affect various immune cells in the liver. Although PIC II has not been shown to have a direct regulatory effect on immune cells, it can alleviate apoptosis and inflammation in sepsis by decreasing the expression of toll-like receptor 4 (TLR4) and tumor necrosis factor-alpha (TNFα) in an ischemic injury rat model [16], thereby reducing the inflammatory response and apoptosis in endothelial cells through the sirtuin 1 (SIRT1)/lectin-like oxLDL receptor-1 (LOX-1) signaling pathway [17]. However, whether PIC II can protect the liver from Mdr2 deficiency-induced liver fibrosis and the potential interaction between PIC II and different immune cells in fibrotic livers remains to be clarified.

In the current study, we hypothesized that PIC II regulates macrophage polarization and function to modulate the behavior and interaction between key immune cells, particularly NK cells and neutrophils, thereby inhibiting the activation of HSCs and alleviating liver fibrosis in $Mdr2^{-/-}$ mice. This hypothesis was tested using transcriptome sequencing analysis and various molecular biology experiments. Our findings not only elucidate how different immune cells regulate the immune microenvironment and HSC activation during the development of liver fibrosis but also propose PIC II as a natural ingredient with potential as a novel therapeutic option for overcoming the challenges of anti-fibrotic treatment.

Materials and Methods

Materials

PIC II (PS0323) was obtained from PUSH BIO-Technology (Chengdu, China). Mouse IL-2, mouse transforming growth factor-β (TGF-β), and mouse IFN-γ (C746) were purchased from Novoprotein Co., Ltd. (Shanghai, China). Lipopolysaccharide (LPS) and other consumables were obtained from Sigma-Aldrich (St. Louis, USA). Antibodies against F4/80 (28463-1-AP), collagen 1 (COL, *Col1a1*, 67288-1-AP), fibronectin (FN, *Fn1*, 15613-1-AP), C-X-C motif chemokine ligand 16 (CXCL16, 60123-1-lg), myeloperoxidase (MPO, 66177-1-Ig), Janus kinase 1 (JAK1, 66466-1-lg), tyrosine kinase 2 (TYK2, 67411-1-lg), PERFORIN (14580-1-AP), GZMB (13588-1-AP), CD11B (66519-1-lg) and *β*-Actin (66009-1-Ig) were obtained from Proteintech (Rosemont, USA). Antibodies against histone H3 (citrulline R2/R8/R17, ab5103) and CD161 (ab197979) were purchased from Abcam (Cambridge, USA). Antibody against alpha-smooth muscle actin (*α*-SMA, 19245S) was obtained from Cell Signaling Technology (Danvers, USA). Antibodies against signal transducer and activator of transcription 1 (STAT1, A12075), p-STAT1 (AP0453), p-JAK1 (AP0530), p-TYK2 (AP0543) and CD68 (A13286) were purchased from ABclonal Technology Co., Ltd. (Wuhan, China). Antibody against CXCR6 (E-AB-11112) was obtained from Elabscience Biotechnology Co., Ltd. (Wuhan, China). Alexa Fluor 594 anti-rabbit IgG secondary antibody (8889S) was purchased from Cell Signaling Technology (Danvers, USA), and Alexa Fluor 488 anti-mouse IgG secondary antibody (A32723) was obtained from Thermo Fisher Scientific (Waltham, USA).

Animal experiments

$Mdr2^{-/-}$ mice (7 weeks old, 20−22 g, both male and female) were housed under pathogen-free conditions in a standard environment with a 12-h light-dark cycle and fed normal chow *ad libitum*. All animal studies and procedures were approved by the Institutional Animal Care and Use Committee of Beijing University of Chinese Medicine and performed in

compliance with all guidelines and regulations (BUCM-4-20200730023160). After a 1-week acclimatization period, the mice were randomly divided into four groups (n = 6): (1) wild type (WT) group; (2) Mdr2$^{-/-}$ group; (3) Mdr2$^{-/-}$ + PIC II low dose (L) group (5 mg·kg^{-1}), and (4) Mdr2$^{-/-}$ + PIC II high dose (H) group (10 mg·kg^{-1}). Mice in groups (1) and (2) were given saline, while mice in groups (3) and (4) received two different doses of PIC II for 14 days. In a macrophage depletion experiment, mice were randomly divided into four groups (n = 6): (1) WT group; (2) Mdr2$^{-/-}$ + empty liposome (Neg) group; (3) Mdr2$^{-/-}$ + clodronate liposome (CL) group; (4) Mdr2$^{-/-}$ + CL + PIC II group (10 mg·kg^{-1}). Mice in group (2) received empty liposomes, while mice in groups (3) and (4) were administered clodronate-liposomes (1 mg·mL^{-1}, 50 μL/mouse, YEASEN, Shanghai, China) through the tail vein once every three days until the day before sacrifice. Mice in group (4) also received 10 mg·kg^{-1} PIC II for 14 days. After the treatment period, all mice were sacrificed to obtain blood and liver samples for subsequent experiments.

Histological and immunofluorescence staining

After fixation in formalin, liver tissues were embedded in paraffin and cut into 5 μm sections for staining. The sections were deparaffinized in xylene and dehydrated in ethanol before being stained using a hematoxylin and eosin (H&E) staining kit and a Masson's staining kit. For immunofluorescence staining, the sections were blocked with 0.2% Triton X-100−2.5% BSA, 1 × phosphate-buffered saline (PBS), and 10% goat serum after undergoing antigen retrieval. The primary antibodies against FN (dilution 1 ∶ 200), α-SMA (dilution 1 ∶ 400), collagen (dilution 1 ∶ 400), F4/80 (dilution 1 ∶ 300), CXCL16 (dilution 1 ∶ 360), CD68 (dilution 1 ∶ 400), MPO (dilution 1 ∶ 400), citrullinated histone H3 (CitH3, dilution 1 ∶ 400), and CD11b (dilution 1 ∶ 400) were incubated overnight at 4 °C. After washing, the sections were incubated with either goat anti-mouse IgG (H + L) highly cross-adsorbed 488 secondary antibody or anti-rabbit IgG (H + L) 594 secondary antibody (Thermo Fisher Scientific, Waltham, USA) and stained with DAPI. Following nuclear staining, the sections were sealed with resin and observed using an Aperio Versa microscope (Leica, Wetzlar, Germany).

RNA-sequencing and bioinformatics analysis

The total RNA from the livers of Mdr2$^{-/-}$ mice was extracted and quantified using a NanoRhatometer$^{@}$ spectrophotometer (IMPLEN, USA). The integrity of the RNA was assessed with an RNA Nano Assay kit, and poly-T oligo-attached magnetic beads were used to purify the mRNA. After synthesizing the cDNA, the AMPure XP system (Beckman Coulter, USA) was employed to purify the library fragments, enriching cDNA fragments of 250−300 bp. The sequencing library was then established using the NEBNext UItra^{TM} RNA Library Prep Kit (NEB) and generated on the Illumina Novaseq platform as previously described [18]. Subsequently, sequencing samples were normalized, and differentially expressed genes (DEGs) were analyzed using edgeR software. Gene ontology (GO) enrichment analysis of DEGs was performed with the clusterProfiler R package. Gene set enrichment analysis (GSEA) and hierarchical clustering analysis were conducted using the heatmap R package. For GSEA, DESeq2 was used as the ranking metric to conduct enrichment analysis (http://software.broadinstitute.org/gsea/index.jsp) to determine whether target genes displayed statistically significant and consistent differences between two biological samples. For weighted gene co-expression network analysis (WGCNA), coding gene expression profiles were used to mine co-expressing genes and co-expression modules. Protein-encoding gene expression profiles were extracted from the COAD expression profiles in the TCGA database, and samples were clustered using hierarchical clustering. Outliers were removed, and the remaining samples were retained. The Pearson correlation coefficient was used to calculate the distance between each gene, and the R software package WGCNA was used to construct a weighted co-expression network.

Cell isolation, culture, and treatment

RAW cells (a macrophage cell line) and LX-2 cells (a hepatic stellate cell line) were cultured in DMEM medium supplemented with 10% Fetal bovine serum (FBS) and incubated at 37 °C with 5% CO_2. For preparing conditioned medium, cellular RNA, and protein, RAW cells were treated with LPS (50 ng·mL^{-1}), IFN-γ (2.5 ng·mL^{-1}), and/or PIC II (5, 10, 20 μmol·L^{-1}) for 24 h. The medium derived from these macrophages was then collected for protein extraction and subsequently used as a conditioned medium (CM-M) for establishing co-culture systems with HSCs, NK cells, and neutrophils. Primary NK cells were isolated from the mouse spleen using the NK extraction kit (P9310) from Solarbio Science & Technology Co., Ltd. (Beijing, China). The cells were pseudo-suspension cultured for about 6 h [19, 20] and then treated with PBS or various CM-Ms. After 24 h of culture, the cells were collected for subsequent experiments. For co-culture experiments involving NK cells and LX-2 cells, HSCs (1 × 10^5 cells per well of a 6-well plate) were pre-treated with TGF-β for 24 h. The isolated NK cells (1 × 10^6 cells per well of a 6-well plate), pre-activated by IL-2 or CM-M for 6 h, were then added at a ratio of 10 ∶ 1 to establish the co-culture system for 24 h [21]. Following this, cells and treatment media were collected for subsequent tests. Primary neutrophils were isolated from mouse bone marrow using a neutrophil extraction kit (P8550-200 mL) from Solarbio. The cells were pseudo-suspension cultured for about 4 h, then treated with LPS (50 ng·mL^{-1}) and/or PIC II (5, 10 and 20 μmol·L^{-1}). After treatment, cell samples were collected for immunofluorescence experiments or RNA extraction. For the co-culture of neutrophils and HSCs, activated HSCs (pre-treated by TGF-β) were co-cultured with isolated neutrophils at a ratio of 1 ∶ 3 with the presence of different doses of PIC II for 24 h [22, 23]. After 24 h, cell samples were collected for protein extraction, RNA extraction, or immunofluorescence analysis.

Transwell assay of NK cells and macrophages

For the Transwell assay of NK cells and macrophages, a total of 1 × 10^5 NK cells were added to the top chamber of the Transwell system (0.4 μm) with 1% FBS DMEM medi-

um, while 1 × 10^5 attached macrophages were added to the lower chamber with 1% FBS DMEM medium. These macrophages were treated with LPS (50 ng·mL^{-1}), IFN-γ (2.5 ng·mL^{-1}), and various doses of PIC II (5, 10, 20 μmol·L^{-1}) for 6 h.

Flow cytometry analysis

For flow cytometry analysis, isolated primary NK cells were co-cultured with TGF-β-treated HSCs at a ratio of 10 ∶ 1 as previously described [21]. After attachment, the co-cultured cells were treated with the conditioned medium of macrophages for 24 h. The cells were then collected, digested without EDTA, and centrifuged at 2000 *g* for 5 min at 4 °C. The fixed cells were first incubated with *α*-SMA antibody (1 ∶ 400) and 5 μL 7-AAD solution from the 7-AAD staining kit (BD Biosciences, CA, USA). For *α*-SMA staining, cells were stained with 4 μmol·L^{-1} Goat anti-Rabbit IgG (H + L) Secondary Antibody Alexa Fluor 488 for 30 min in the dark at room temperature and further stained with 7-AAD binding provided by the staining kit. The *α*-SMA/7-AAD signal was then detected using a CytoFLEX flow cytometer (Beckman Coulter, Pasadena, CA), and FlowJo software (v.10.3) was used for subsequent data analysis.

Statistical analysis

All data were repeated at least three times and are presented as mean ± SEM. Statistical analysis was conducted using one-way ANOVA in GraphPad Prism version 8.0. Statistical significance was considered at a P value of ≤ 0.05.

Additional method information and details are provided in the Supplementary files.

Results

PIC II significantly alleviates hepatic fibrosis in Mdr2$^{-/-}$ mice

To broadly analyze the potential pharmacological effects of PIC II on hepatic fibrosis, we utilized Mdr2$^{-/-}$ mice, which mimic the immunopathogenesis and symptoms of patients with liver fibrosis (Fig. 1A, left panel). As shown in Fig. 1A, right panel and Fig. S1A, there was little difference in weight loss, or the ratio of liver or spleen to body weight among the different groups. We further applied H&E and Masson's trichrome staining to evaluate pathological changes before and after PIC II administration. Obvious inflammatory infiltration, extracellular matrix (ECM) deposition, and fibrous scarring were observed in the liver of Mdr2$^{-/-}$ mice, but these symptoms were markedly alleviated by different doses of PIC II to varying degrees (Fig. 1B). Consistently, although PIC II had less effect on *γ*-glutamyl transpeptidase (*γ*-GGT, a cell surface enzyme indicating hepatobiliary injury, Fig. S1B), it significantly downregulated the serum levels of aspartate aminotransferase (AST) and alanine aminotransferase (ALT), total biliary acid (TBA), total bilirubin (TBIL), and alkaline phosphatase (ALP) in a dose-dependent manner. These markers reflect bile acid accumulation and liver fibrosis severity induced by the deficiency of Mdr2 (Fig. 1C and Fig. S1B). To elucidate the protective effects and underlying mechanisms of PIC II, we performed RNA-sequencing analysis of fibrotic livers in Mdr2$^{-/-}$ mice and plotted DEGs implicated in fibrosis-related genes as a heatmap (Fig. 1D). A total of 8274 DEGs was identified among the three different groups. In cluster 1, the expression of genes such as *Stat3*, ribosomal protein S6 (*Rps6*), and small mother against decapentaplegic family member 3 (*Smad3*) was downregulated in the Mdr2$^{-/-}$ mice and further decreased in the Mdr2$^{-/-}$ + PIC II group. These genes are often elevated early and sustained in liver injury. In cluster 2, the expression of genes was upregulated in the Mdr2$^{-/-}$ group and further increased in Mdr2$^{-/-}$ + PIC II group, including key genes involved in inhibiting hepatic stellate cell (HSC) proliferation and activation like peroxisome proliferator-activated receptor gamma (*Pparg*) and *Smad7* as well as collagen degradation-related gene such as matrix metallopeptidase 13 (*Mmp13*). In cluster 3, genes like cellular communication network factor 2 (*Cnn2*) and collagen formation genes in cluster 4, including tissue inhibitor of metalloproteinase 1 (*Timp1*) and collagen type XXIII alpha 1 chain (*Col23a1*), were remarkably downregulated in the Mdr2$^{-/-}$ + PIC II group compared to the Mdr2$^{-/-}$ group

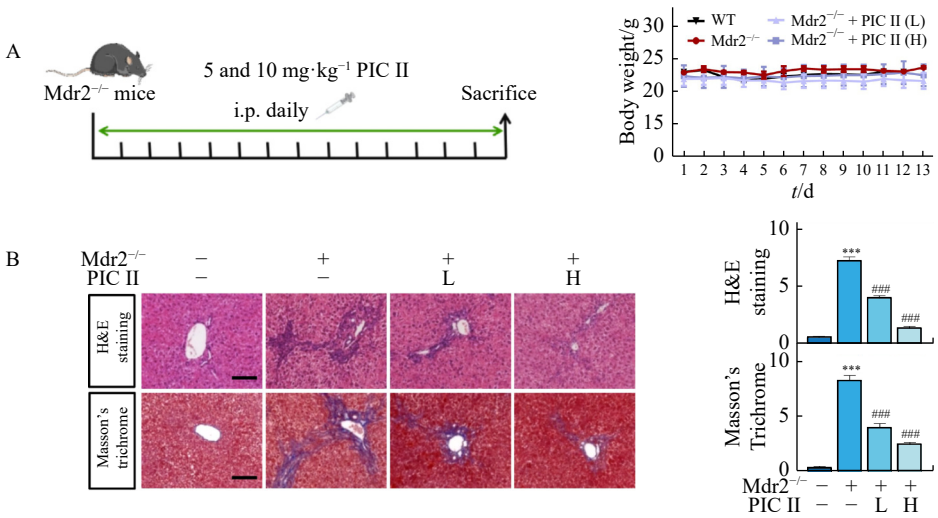

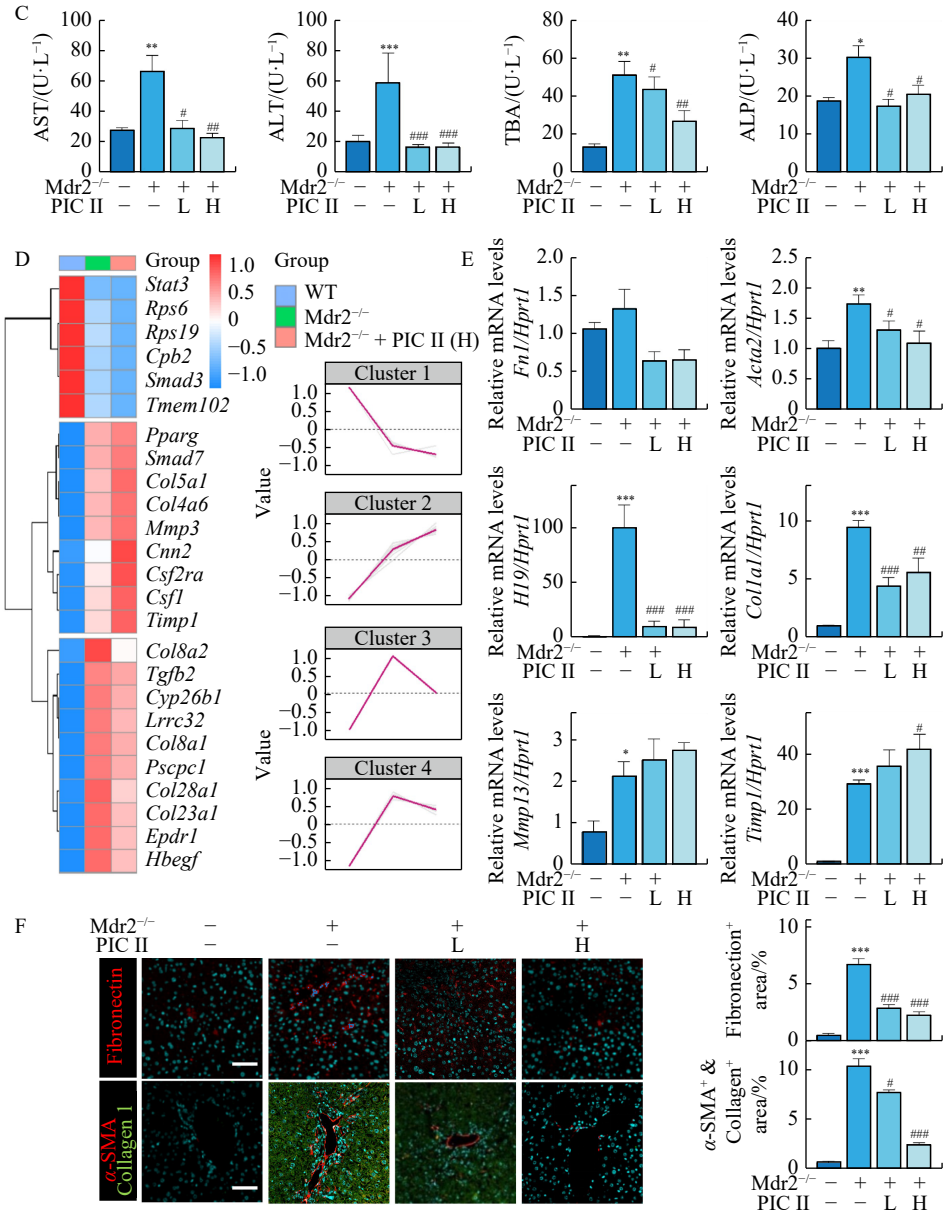

Fig. 1 PIC II alleviates hepatic fibrosis in Mdr2$^{-/-}$ mice. (A) Flowchart of the animal experiment and body weight changes of different groups. (B) Representative images of H&E staining and Masson trichome's staining. Quantifications were performed using Image J (Scale bar = 20 μm). (C) Serum levels of ALT, AST, TBA, and AKP. (D) The heatmap and clusters of liver fibrosis-related markers. (E) Relative mRNA levels of *Fn1*, *Acta2*, *H19*, *Col1a1*, *Mmp13*, and *Timp1* were measured by qPCR and further normalized with *Hprt1*. (F) Representative images of immunofluorescence staining for Fibronectin, *α*-SMA, and Collagen 1 in the liver. Quantifications were performed using Image J (Scale bar = 20 μm). Data are presented as the mean ± SEM (n = 6). Statistical significance: $^{*}P < 0.05$, $^{**}P < 0.01$, $^{***}P < 0.001$ *vs* the WT group; $^{\#}P < 0.05$, $^{\#\#}P < 0.01$, $^{\#\#\#}P < 0.001$ *vs* the Mdr2$^{-/-}$ group.

(Fig. 1D). Consistently, the real-time polymerase chain reaction (RT-PCR) results validated the mRNA changes of representative fibrosis-related genes in the heatmap, showing that PIC II mainly inhibited the expression of collagen-synthesis-related genes [*Fn1*, actin alpha2 (*Acta2*), *H19* and *Col1a1*] while positively supporting collagen-degradation pathways (increased *Mmp13* and *Timp1*, Fig. 1E). Furthermore, immunofluorescence staining confirmed the anti-fibrotic effects of PIC II in the Mdr2$^{-/-}$ mouse model, as illustrated by the reduced distribution of Fibronectin, *α*-SMA and Collagen1 (Fig. 1F and Fig. S1C). Notably, PIC II had no obvious effect on the cell viability of aHSCs directly (both HSC cell lines and primary HSCs, Figs. S2A and S2B) and did not observably downregulate the protein levels of *α*-SMA and Fibronectin except for Collagen 1 in aHSC (Fig. S2C), suggesting that PIC II might exert a suppressive effect on aHSCs through an indirect mechanism.

PIC II may attenuate hepatic fibrosis by improving hepatic immune microenvironment in Mdr2$^{-/-}$ mice

To investigate whether the anti-fibrotic effects of PIC II

are reliant on the regulation of different immune cells, we systematically analyzed the RNA-sequencing data to identify primary target genes influenced by PIC II. Using the differentiated modules of all DEGs, we employed WGCNA to construct a gene co-expression network. The Pearson's correlation coefficient was applied to cluster the samples, resulting in the identification of eight modules through hierarchical clustering of the predetermined dissimilarities (Fig. 2A). To identify liver fibrosis-related modules, we examined the relationship between these modules and hepatic pathology and function. Among the eight modules, the turquoise and blue modules were highly associated with pathological manifestations and were thus selected for further analysis. Additionally, three co-expression modules—related to inflammatory infiltration, collagen deposition, and oxidative stress—were primarily enriched, with inflammatory infiltration playing a significant role in governing liver fibrosis (Fig. 2B). Given these findings, we speculated that PIC II might exert its potential effects through immune cells. We plotted DEGs implicated in immune-related targets as a heatmap and prepared relative clusters (Fig. 2C). Compared with the WT group, most differential genes were enriched in cluster 3, which were upregulated in both the model and PIC II-treated mice. These included macrophage markers Dendritic Cells Maturation (*Cd86*), colony-stimulating factor 2 receptor subunit alpha (*Csf2ra*) and *Csf3r*, as well as NK cell activation cytokines like C-C motif chemokine ligand 3 (*Ccl3*) and interleukin 4 receptor alpha (*Il4ra*). Additionally, the upregulated NK cell markers—such as killer cell lectin-like receptor subfamily A member 8 (*Klra8*), *Cd226* and natural cytotoxicity triggering receptor 1 (*Ncr1*)—and the downregulated neutrophil markers—such as *Cd66*, lymphocyte antigen 6 family member G (*Ly6g*), and C-X-C motif chemokine receptor 1 (*Cxcr1*) in PIC II-treated mice further indicated the enrichment of immune cells (Fig. 2C, Figs. S3A and S3B). Given the notable changes in immune reactions, we analyzed different immune cell subtypes across the three groups and found that PIC II significantly affected the proportion of macrophages (Fig. 2D). Generally, M1 macrophages are known to stimulate inflammatory reactions, whereas M2 macrophages contribute to the remission of liver fibrosis [24]. Notably, further quantitative analysis revealed that PIC II increased the numbers of M1 macrophages and monocytes but did not decrease the number of M2-type macrophages and NK cells compared with Mdr2$^{-/-}$ mice (Figs. 2E and 2F). These results suggest that PIC II may alleviate fibrosis by establishing intricate links among diverse immune cells, indicating a far more complex mechanism than traditionally imagined.

PIC II enhances the function of M1-polarized macrophages and promotes the release of chemokine CXCL16

Recently, M1-polarized macrophages have been shown to ameliorate liver fibrosis by modulating the immune microenvironment in carbon tetrachloride (CCl_4)- and bile duct ligation (BDL)-induced liver fibrosis models [25]. Hence, we investigated whether and how PIC II regulates genes involved in macrophage function and polarization. According to the heatmap shown in Fig. 3A, DEGs enriched in macrophage-related modules, particularly M1-polarized macrophage-related pathways, were significantly altered in the Mdr2$^{-/-}$ + PIC II group compared with the Mdr2$^{-/-}$ group. In cluster 1, the expression of genes was upregulated in the Mdr2$^{-/-}$ group but decreased in the Mdr2$^{-/-}$ + PIC II group, including spondin 2 (*spon2*) and *ccl5*, as well as other cell adhesion-related genes. Notably, the expression of genes in cluster 3, mainly associated with M1-polarized macrophages, was upregulated in the Mdr2$^{-/-}$ + PIC II group. These genes included those related to the chemotactic ability of activated M1 macrophages, such as *Cd80*, *Cxcl16*, and nitric oxide synthase 2 (*Inos*, *Nos2*). Interestingly, *cd163* in cluster 4 indicated enhanced phagocytosis accompanying increased macrophage activity. Consistent GSEA plot results also demonstrated that DEGs enriched in M1-polarized macrophage marker genes were significantly upregulated in the Mdr2$^{-/-}$ + PIC II group compared to the Mdr2$^{-/-}$ group (Fig. 3B). Our qPCR results in Fig. 3C showed that macrophages in the fibrotic liver of mice did not appear to be polarized into an inflammatory state, as PIC II did not significantly upregulate inflammatory markers such as *il6* and *inos*, but slightly increased *Cd163* and decreased the M2-type macrophage maker transglutaminase 2 (*Tgm2*). Meanwhile, the expression of *Mmp13* and *Mmp2* was significantly upregulated after PIC II treatment, consistent with the downregulated fibronectin 1 (*Fn1*) (Fig. 3D). Interestingly, among the different subsets of changed chemokines listed in Fig. 3A, *Cxcl16*, *Cxcl1*, *Cxcr2*, and *Ccl5* were detected by qPCR, with *cxcl16* showing clear upregulation in the Mdr2$^{-/-}$ + PIC II group compared to the WT group Fig. 3D and Fig. S4A. Consistently, PIC II markedly enhanced the hepatic expression and intrahepatic distribution of CXCL16, primarily located around macrophages as indicated by positive staining of the macrophage marker F4/80, in the liver of Mdr2$^{-/-}$ mice (Fig. 3E and Fig. S4B). We also confirmed that PIC II at different dosages dramatically increased the cellular level of chemokine CXCL16 in M1-type macrophages induced by the administration of IFN-γ and LPS (Figs. 3F−3H) and promoted its secretion into the cell culture medium (CM) (Figs. 3H, 3I and Fig. S4C). Collectively, these findings suggest that PIC II promotes M1-polarized macrophages and triggers the secretion of CXCL16 in macrophages in Mdr2$^{-/-}$ mice. Since the CM from CXCL16 highly expressed M1 macrophages did not show a significant inhibitory effect on HSC activation (Fig. S4D), we shifted our focus to explore other mechanisms by which M1 macrophages might affect the liver fibrosis process.

PIC II promotes the M1 polarization of CXCL16-expressed macrophages accompanied by the activation and recruitment of NK cells

Although PIC II did not visibly impact the dominant

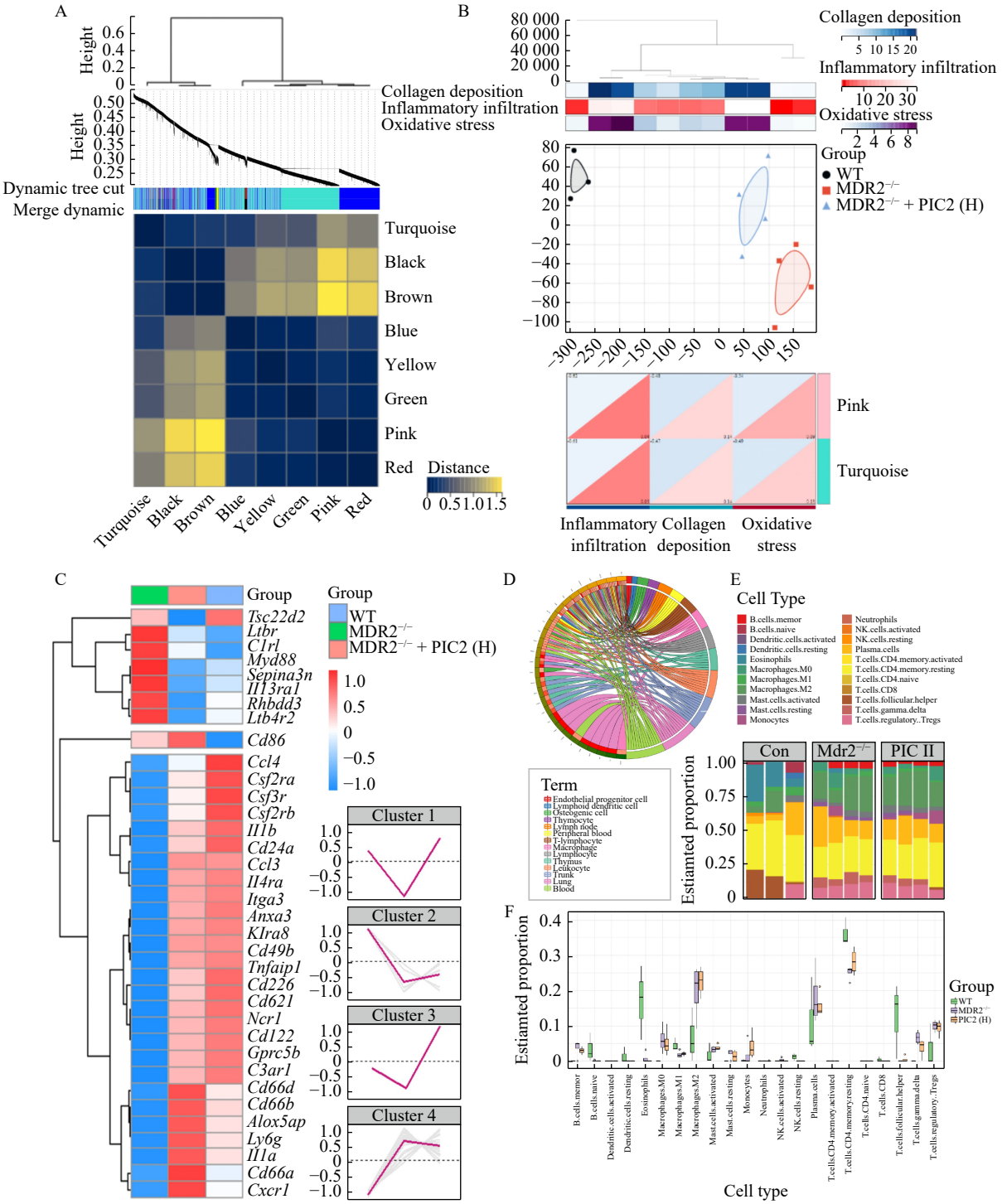

Fig. 2 PIC II attenuates hepatic fibrosis by improving immune-related DEGs in Mdr2$^{-/-}$ mice. (A) WGCAN plots of RNA-seq analysis. (B) Gene co-expression analysis of the inflammatory infiltration, oxidative stress, and collagen deposition in different groups of mice. (C) The heatmap and clusters of liver fibrosis- and inflammation-related markers. (D) Dominant cells analysis in the liver of mice. (E) Proportion of immune cell subtypes. (F) CIBERSORT analysis of multiple immune cell subtypes in the liver of mice.

population of NK cells, the heatmap results in Fig. 4A revealed that DEGs enriched in inflammatory cytokines, especially markers of NK cells such as interferon-gamma receptor (*Ifngr*), neural cell adhesion molecule 1 (*Ncam1*), integrin subunit alpha 1 (*Itga1*), and NK cell-mediated target cell killing pathways like *Gzmb*, were altered after PIC II administration. Similar results from Gene Set Enrichment Analysis (GSEA) plots confirmed that DEGs enriched in NK cells-mediated immune responses were significantly downregulated in the Mdr2$^{-/-}$ group but were increased with PIC II administra-

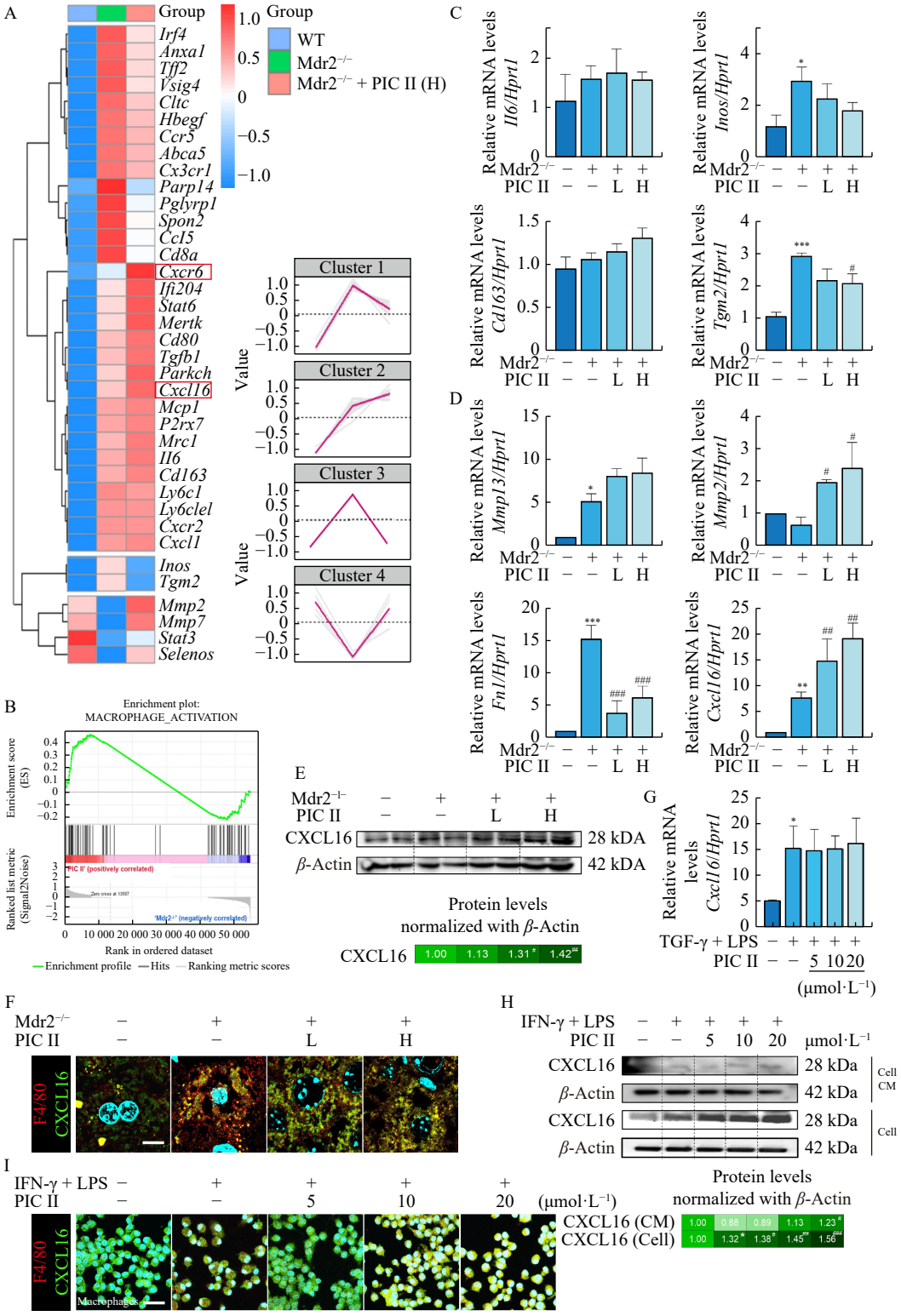

Fig. 3 PIC II enhances the function of M1-polarized macrophages and promotes the release of chemokine CXCL16. (A) The heatmap and clusters of M1 type-related macrophage markers. (B) GSEA analysis of M1-polarized macrophage activation. Relative mRNA levels of (C) *Il6*, *Inos*, *Cd163*, *Tgm2*, (D) *Mmp13*, *Mmp2*, *Fn1*, and *Cxcl16* in mice liver tissue were measured by qPCR and further normalized with *Hprt1*. (E) The protein levels of CXCL16 were measured by Western blotting analysis and normalized by *β*-Actin in the mouse liver. Relative mRNA levels of (G) *Cxcl16* in macrophages were measured by qPCR and further normalized with *Hprt1*. (H) The protein levels of CXCL16 in macrophages and derived CM were measured by Western blotting analysis and normalized by *β*-Actin. Representative images of immunofluorescence staining for F4/80 and CXCL16 (F) in the liver (Scale bar = 20 μm) and (I) macrophages (Scale bar = 100 μm). Data are presented as the mean ± SEM ($n = 6$). Statistical significance: $^{*}P < 0.05$, $^{**}P < 0.01$, $^{***}P < 0.001$ *vs* the control group; $^{\#}P < 0.05$, $^{\#\#}P < 0.01$, $^{\#\#\#}P < 0.001$ *vs* the model group.

tion (Fig. 4B). Additionally, PIC II slightly increased or maintained the expression of PERFORIN and GZMB (cytotoxic factors released by NK cells), and notably increased the expression of CXCR6 (the surface receptor of NK cells) and the apoptosis-inducing factor STAT1 in the Mdr2$^{-/-}$ mice (Fig. 4C and Fig. S5A). Considering the recruitable feature of NK cells and the interaction between immune cells in liver fibrosis, we constructed a co-culture system of macrophages and NK cells to explore how M1 polarized macrophages might regulate NK cell activity in Mdr2$^{-/-}$ mice. Briefly, M1-type macrophages induced by IFN-γ plus LPS were seeded in the lower chamber, and primary NK cells were plated in the upper transwells (Fig. 4D). As expected, the transwell migration assay demonstrated that, after being treated with PIC II, CM-M promoted the recruitment of NK cells (Fig. 4E). Similarly, immunofluorescence co-staining of CD161 (NK1.1) and CXCL16 confirmed that PIC II at different dosages increased the expression of CXCL16 in co-cultured NK cells (Fig. 4F and Fig. S5B), even without significantly upregulating cytotoxic factors PERFORIN and GZMB. Previous studies have demonstrated the multiple roles of CXCR6 in HSC activation, fibrogenesis, and proliferation, and the activation of NK cells might lead to HSC apoptosis [25]. Therefore, we investigated whether CXCL16 released from PIC II-treated macrophages could be recognized by CXCR6 expressed on NK cells. The relative mRNA and protein levels of *Cxcr6* were increased after PIC II administration in the livers of Mdr2$^{-/-}$ mice (Fig. 4G, left panel) and in co-cultured NK cells (Figs. 4G, right panel and 4H). These results suggest that PIC II promotes M1 polarization of CXCL16-expressing macrophages, accompanied by the recruitment and activation of NK cells, potentially driven by the CXCL16-CXCR6 pathway.

PIC II facilitates the cytotoxicity of NK cells and promotes the apoptosis of HSCs

To further elucidate whether NK cells activated by macrophages could kill aHSCs, we isolated primary NK cells from the spleens of mice. These NK cells were pre-treated with IL-2 and/or CM-M containing different doses of PIC II and then co-cultured with TGF-β-induced aHSCs at a 10 ∶ 1 ratio (Fig. 5A). The purity and activity of NK cells (marked by CD16, CD56, and CD161) isolated from mice were confirmed (Figs. S6A and S6B). As shown in Fig. 5B, the viability of co-cultured cells in the model group and PIC II CM-treated group was significantly decreased. Additionally, the mRNA levels of fibrosis-related genes (*Acta2*, *Col1a1*, and *Fn1*) in co-culture cells were markedly decreased in the presence of PIC II-treated NK cells (Fig. 5C). PIC II was shown to increase the cytotoxicity of NK cells towards aHSCs to varying degrees, verified by the increased mRNA levels of apoptosis-related gene [BCL2-associated X protein (*Bax*), *Caspase 1*, *Caspase 3* and *Caspase 8*] (Fig. S7A). Flow cytometry analysis further confirmed these results, with cells stained for both α-SMA (indicating HSC activation) and 7-AAD (indicating apoptosis). As shown in Fig. 5D, compared to the model group, PIC II increased HSC death marked by both α-SMA and 7-AAD in a dose-dependent manner. The proportion of apoptotic aHSCs in co-culture cells after CM treatment was 9.88%, and in PIC II-treated groups, it was

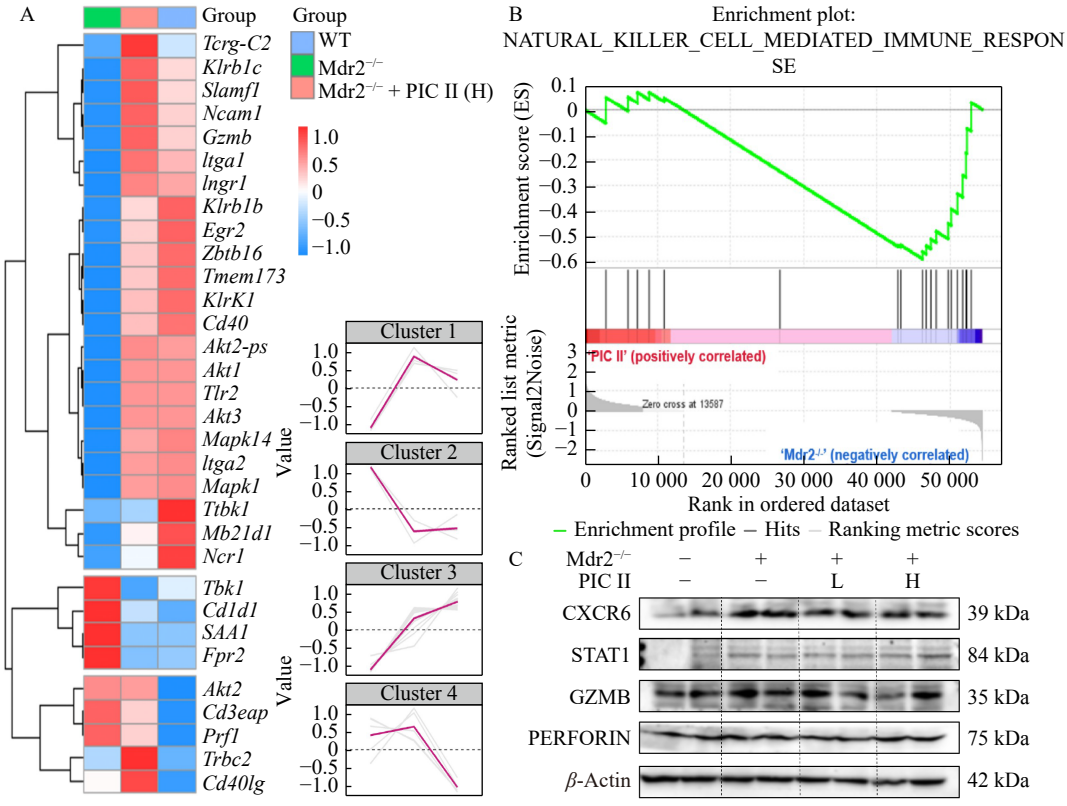

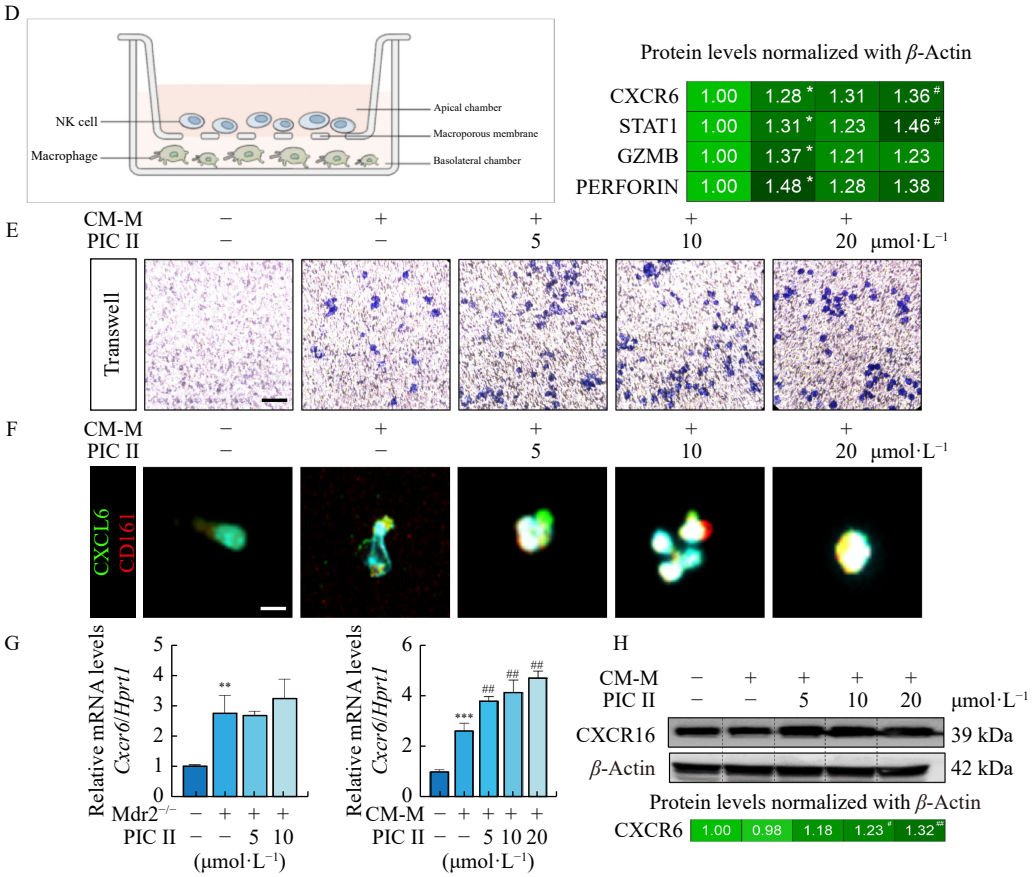

Fig. 4 PIC II promotes CXCL16-expressed M1 macrophages to recruit and activate NK cells. (A) The heatmap and clusters of NK cell-related markers. (B) GSEA analysis of NK cell-mediated immune response. (C) The protein levels of CXCR6, STAT1, GZMB, and PERFORIN were measured by Western blotting analysis and normalized by *β*-Actin in the mice liver. Quantifications were performed using Image J. (D) Schematic of transwell co-culture system of macrophages and NK cells. (E) Representative transwell images of primary NK cells. (F) Representative images of immunofluorescence staining for CD161 and CXCL16 in the primary NK cells (Scale bar = 100 μm). (G) Relative expression of mRNA levels of *Cxcr6* was measured by qPCR and further normalized with *Hprt1* in the liver and co-cultured NK cells. (H) The protein level of CXCR6 was measured by Western blotting analysis and normalized by *β*-Actin in the co-cultured NK cells. Data are presented as the mean ± SEM (*n* = 6). Statistical significance: $^{*}P < 0.05$, $^{**}P < 0.01$, $^{***}P < 0.001$ *vs* the control group; $^{\#}P < 0.05$, $^{\#\#}P < 0.01$ *vs* the model group.

10.36%, 16.34%, and 19.15%, respectively, compared with the apoptosis proportion of 0.13% in the control group. Furthermore, immunofluorescence staining results showed that CM-M containing different doses of PIC II significantly reduced the expression of *α*-SMA in the co-culture of HSC-NK cells (Fig. 5E). After confirming that the activation and viability of HSCs could be inhibited by NK cells recruited by M1 macrophages, we aimed to further explore the underlying mechanisms among these immune cells and HSCs.

Notably, NK cells can suppress aHSC populations by directly killing activated or senescent HSCs. However, the direct cytotoxicity of NK cells on HSCs was not significantly upregulated as expected (Fig. S7B). On the other hand, the inhibitory effects of NK cells on HSCs also rely on the IFN-γ-related network. Interestingly, we observed a significant upregulation of *Ifng* following PIC II administration both in the livers of Mdr2$^{-/-}$ mice (Fig. 6A) and in the co-culture system of HSCs and NK cells (Fig. 6B). Indeed, the interaction of IFN-γ and its receptor at the cell surface was reported to lead the activation of JAK1 and TYK2, resulting in the phosphorylation and nuclear translocation of STAT1 and directly lead to the transcription of genes involved in cell apoptosis [26]. As shown in Fig. 6C, compared with the Mdr2$^{-/-}$ mice, the phosphorylation of Jak1, Tyk2, and their downstream factor STAT1 was upregulated in mouse liver after treatment with different doses of PIC II. Notably, phosphorylated STAT1 primarily translocated to the nucleus after PIC II administration, suggesting that NK cells likely exert an inhibitory effect on aHSCs mediated by the release of IFN-γ. To verify this hypothesis, we used the co-culture system as described in Fig. 5A. Consistently, the *Ifng* level in NK cells was upregulated by PIC II (Fig. 6B), followed by the increased phosphorylation of Jak1, Tyk2, and STAT1 in co-cultured HSCs and NK cells, with STAT1 translocating to the nucleus (Fig. 6D). These results suggest that PIC II enhances the cytotoxicity of NK cells and promotes the apoptosis of aHSCs, potentially relying on the activation of the IFN-γ-Jak1/Tyk2-STAT1 signaling pathway.

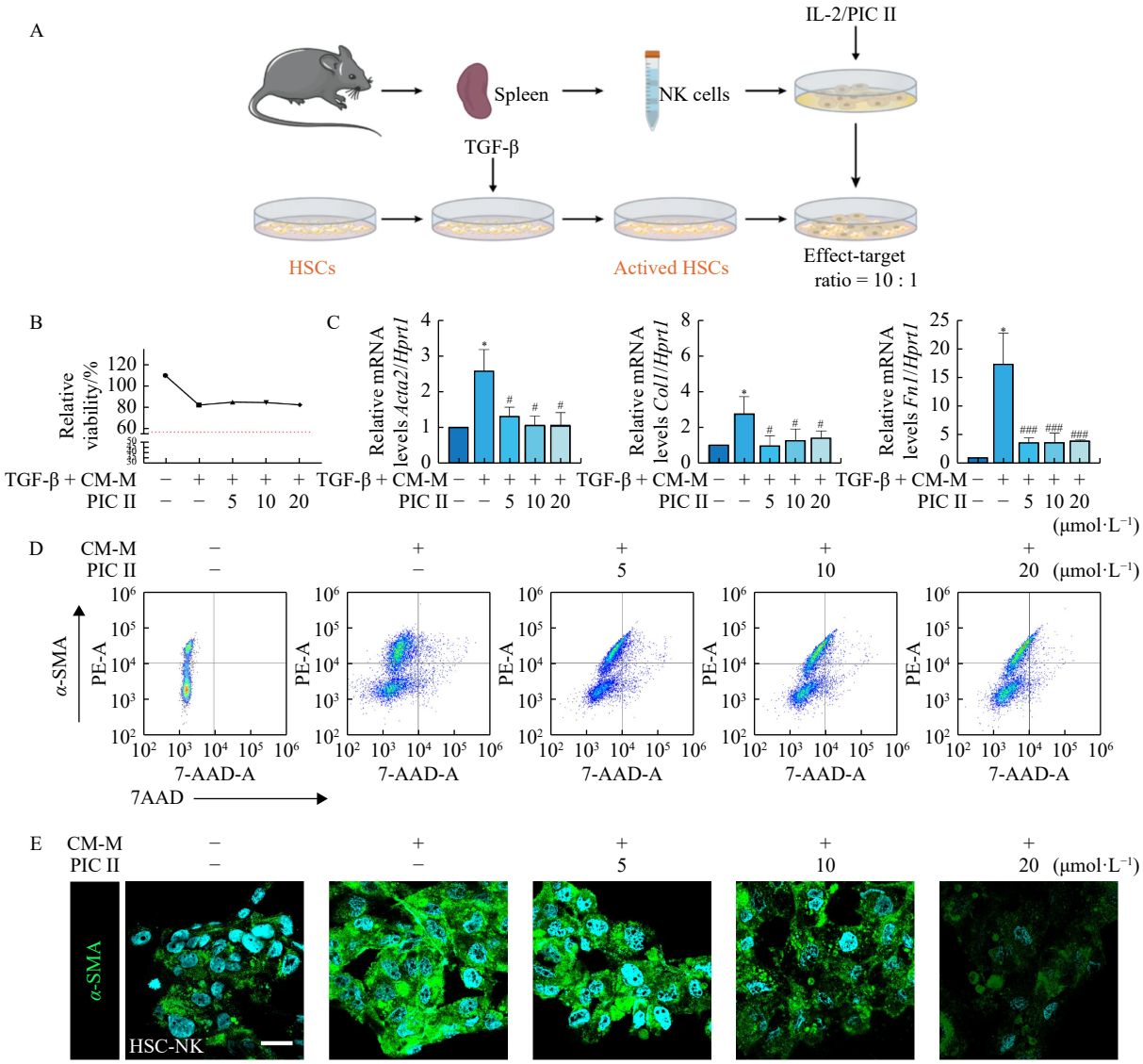

Fig. 5 CM secreted by M1-type macrophages containing PIC II facilitates NK cells to promote the apoptosis of HSCs. (A) Flow chart of the primary NK cells co-cultured with HSCs. (B) CCK-8 results. (C) Relative mRNA levels of *Acta2*, *Col1a1*, and *Fn1* were measured by qPCR and further normalized with *Hprt1* in the co-culture cells. (D) Flow cytometry of 7-AAD and *α*-SMA and (E) representative images of immunofluorescence staining for *α*-SMA in the co-culture of primary NK cells and HSCs (Scale bar = 100 μm). Data are presented as the mean ± SEM ($n = 3$). Statistical significance: $^{*}P < 0.05$ *vs* the control group; $^{\#}P < 0.05$, $^{\#\#\#}P < 0.001$ *vs* the model group.

PIC II inhibits the neutrophil extracellular trap (NET) formation and downregulates the activation of HSCs

Considering the crucial role of intercellular communication between immune cells and HSCs played in liver fibrosis, we further investigated whether PIC II influenced neutrophils, another important cell type in the hepatic immune microenvironment. First, we conducted GSEA plots and found that DEGs associated with neutrophil inhibition were significantly increased in the Mdr2$^{-/-}$ + PIC II group compared to the Mdr2$^{-/-}$ group (Fig. 7A). Based on RNA sequencing results, the expression of DEGs enriched in integrins and cytokines was presented as a heatmap with four clusters identified by hierarchical cluster analysis. As shown in Fig. 7B, PIC II markedly decreased the levels of neutrophil chemotaxis markers (*Cxcl1*, *Cxcl2*) and notably increased the level of the neutrophil senescence marker *Cxcr4*. Additionally, PIC II decreased the levels of neutrophil markers such as lymphocyte antigen 6 complex, locus G (*Ly6g*), *Ly6g5b*, and *Ly6g6d*. These results suggested that PIC II might not only recruit NK cells *via* the CXCL16-CXCR6 axis but also accelerate the senescence of neutrophils. This broadens the possibility of interactions among distinct immune cells in the liver fibrosis process, indicating a complex network of cellular interrelations facilitated by PIC II in modulating the hepatic immune environment.

Another notable aspect is that neutrophil-derived fibrous networks, known as NETs, often exacerbate immune and microvascular conditions, leading to progressive hepatic

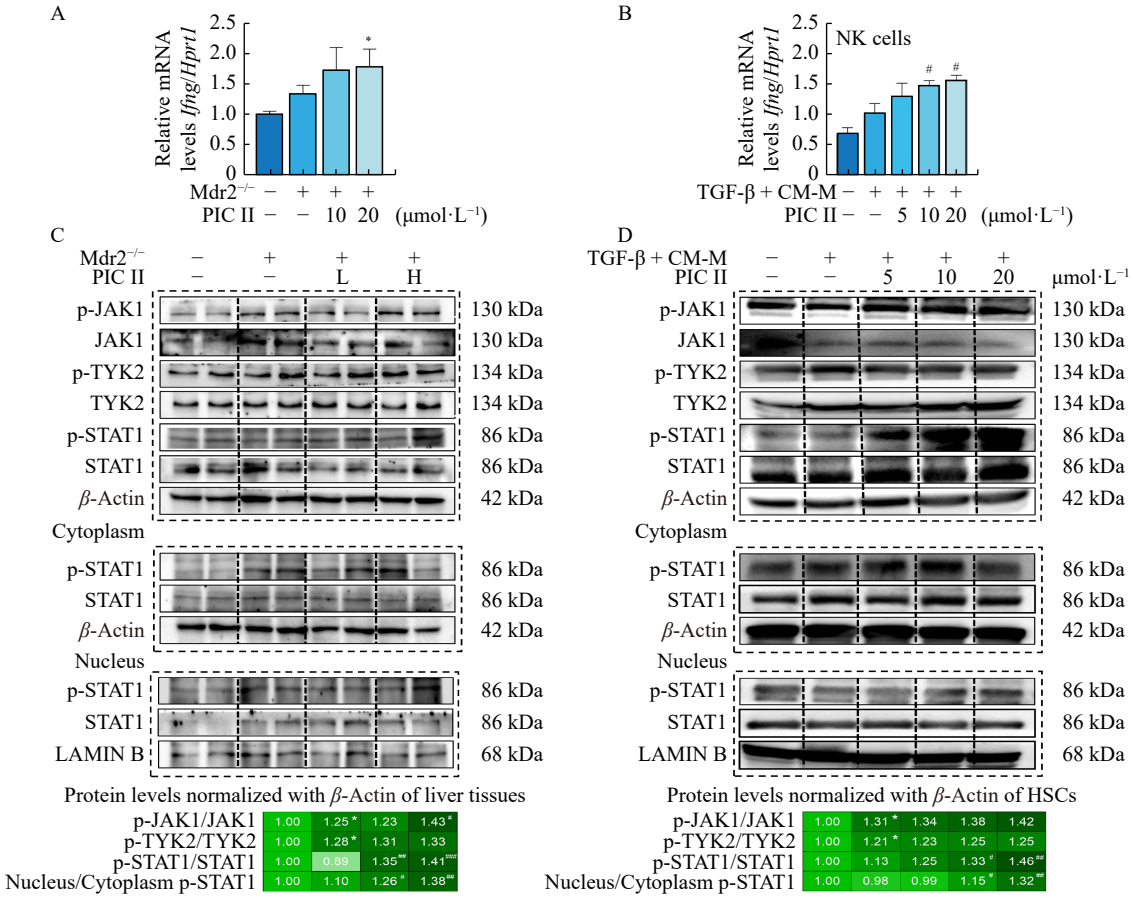

Fig. 6 PIC II enhances the killing effects of NK cells on HSCs *via* the IFN-γ-Jak1/Tyk2-STAT1 pathway. Relative mRNA levels of *Ifn*-γ were measured by qPCR and further normalized with *Hprt1* in (A) mice and (B) primary NK cells. The protein levels of p-JAK1, JAK1, p-TYK2, TYK2, p-STAT1, and STAT1 were measured by Western blotting analysis and normalized by *β*-Actin in the nucleus and cytoplasm of (C) mice liver tissues and (D) co-culture system of NK cells and HSCs. Quantifications were performed using Image J. Data are presented as the mean ± SEM (n = 3). Statistical significance: $^{*}P < 0.05$ *vs* the WT group; $^{\#}P < 0.05$, $^{\#\#}P < 0.01$, $^{\#\#\#}P < 0.001$ *vs* the model group.

fibrosis. To investigate this, we performed immunofluorescence staining for NET markers, CitH3, and MPO, and found that PIC II significantly reduced the formation of extracellular NETs in Mdr2$^{-/-}$ mice (Fig. 7C and Fig. S8). Similarly, the serum level of MPO (Fig. 7D) and the relative mRNA levels of neutrophil-associated genes, such as *Ly6g*, were dramatically increased in the Mdr2$^{-/-}$ group. Interestingly, PIC II markedly decreased MPO levels and intercellular adhesion molecule 1 (*Icam1*) mRNA expression while enhancing the expression of the neutrophil senescence marker *Cxcr4* in the fibrotic liver, with no change in *Ly6g* level (Fig. 7E). Considering the inflammatory crosstalk between neutrophils and HSCs in hepatic fibrosis, we further explored the effects of PIC II on primary activated neutrophils and the co-culture system of neutrophils and HSCs. Consistently, PIC II significantly reduced the formation of NETs induced by IL-2, a classical activator of neutrophils (Fig. 7F), and dose-dependently inhibited the activation of HSCs in the presence of conditioned medium from PIC II-treated neutrophils (CM-Neu) (Fig. 7G). These results suggest that the inhibitory effects of PIC II on aHSCs might also be attributed to the restriction of NET formation, highlighting a potential mechanism by which PIC II mitigates hepatic fibrosis through the modulation of neutrophil activity and NET production.

Depletion of macrophage partially neutralizes the anti-fibrotic effect of PIC II

Based on the vital role that macrophages play in the fibrotic liver of Mdr2$^{-/-}$ mice, we investigated whether the depletion of macrophages would obstruct the hepatoprotective effects induced by PIC II. CL, a classical scavenger agent targeting macrophages, was used for macrophage depletion in Mdr2$^{-/-}$ mice treated with or without PIC II (Fig. 8A). Compared with the Mdr2$^{-/-}$ group, CL markedly increased the levels of TBA, TBIL, AST, ALT, and γ-GGT in serum, which were almost unchanged or only slightly decreased in the Mdr2$^{-/-}$ + CL + PIC II group (Fig. 8B and Fig. S9A). We further evaluated pathological changes after macrophage clearance and observed similar patterns of inflammatory infiltration, ECM deposition, and fibrous scarring in both the Mdr2$^{-/-}$ + CL + PIC II group (Fig. 8C). Additionally, CXCL16 levels decreased and did not co-locate with F4/80, with a slight decrease in NET formation in both the Mdr2$^{-/-}$ +

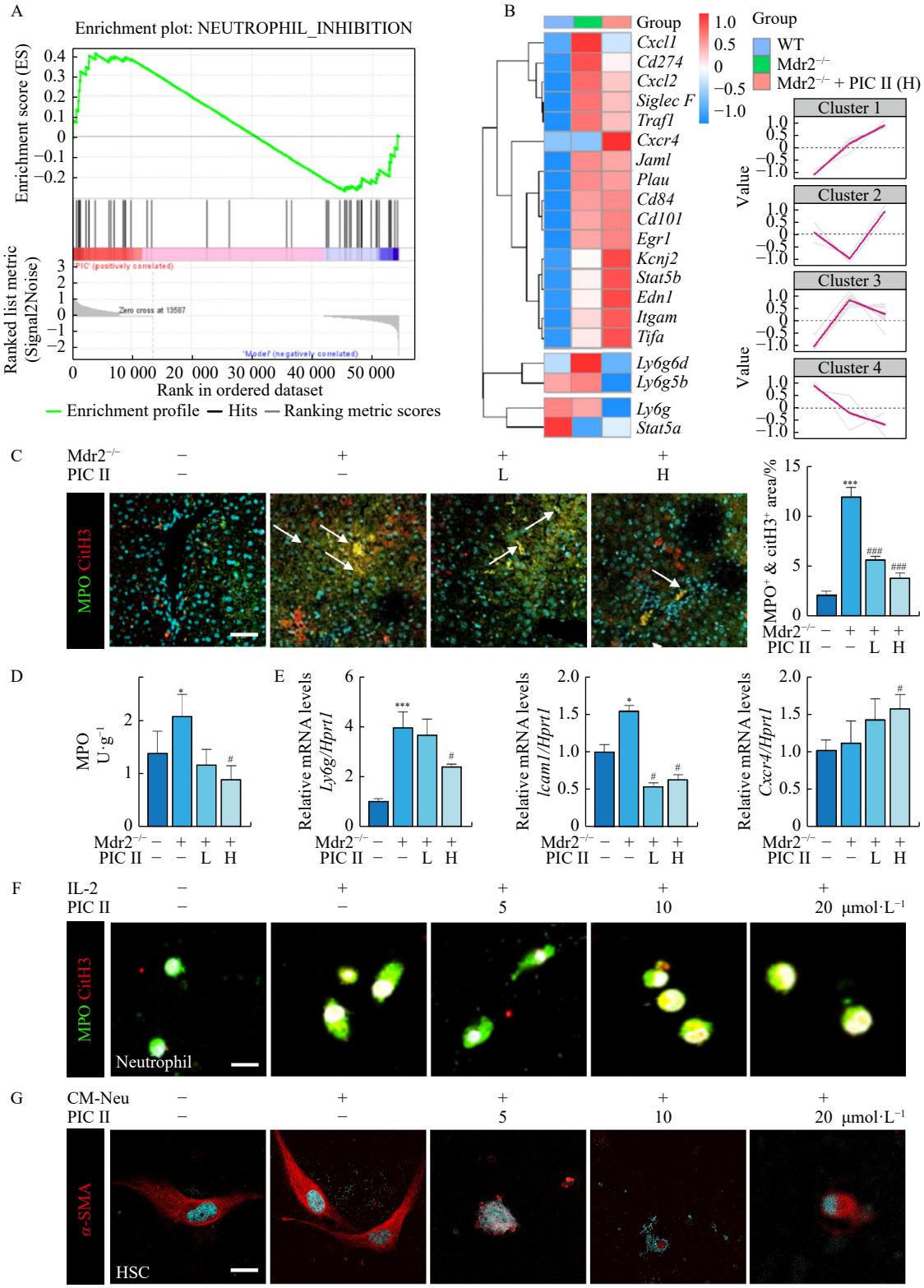

Fig. 7 PIC II inhibits the NET formation and promoted the rupture of aHSCs to alleviate liver fibrosis. (A) GSEA analysis of neutrophil inhibition. (B) The heatmap and clusters of neutrophils-related markers. (C) Representative images of immunofluorescence staining for MPO and CitH3 in the mice liver. Quantifications were performed using Image J (Scale bar = 20 μm). (D) MPO activity. (E) Relative mRNA expression levels of *Ly6g*, *Icam1*, and *Cxcr4* in mice liver were measured by qPCR and further normalized with *Hprt1*. Representative images of immunofluorescence staining for (F) MPO and CitH3 in the primary neutrophils and for (G) *α*-SMA in the HSCs treated with PIC II and CM-Neu (Scale bar = 100 μm). Data are presented as the mean ± SEM ($n = 3$). Statistical significance: $^{*}P < 0.05$, $^{***}P < 0.001$ *vs* the control group; $^{\#}P < 0.05$, $^{\#\#\#}P < 0.001$ *vs* the model group.

CL group and Mdr2$^{-/-}$ + CL + PIC II group (Fig. 8D). To better understand the potency and mechanisms of PIC II after macrophage depletion, qPCR was performed to assess the gene expression of interest. Although the mRNA levels of *Cxcl16* remained similar before and after CL treatment, the typical marker of M1 polarized macrophages, *Inos*, was

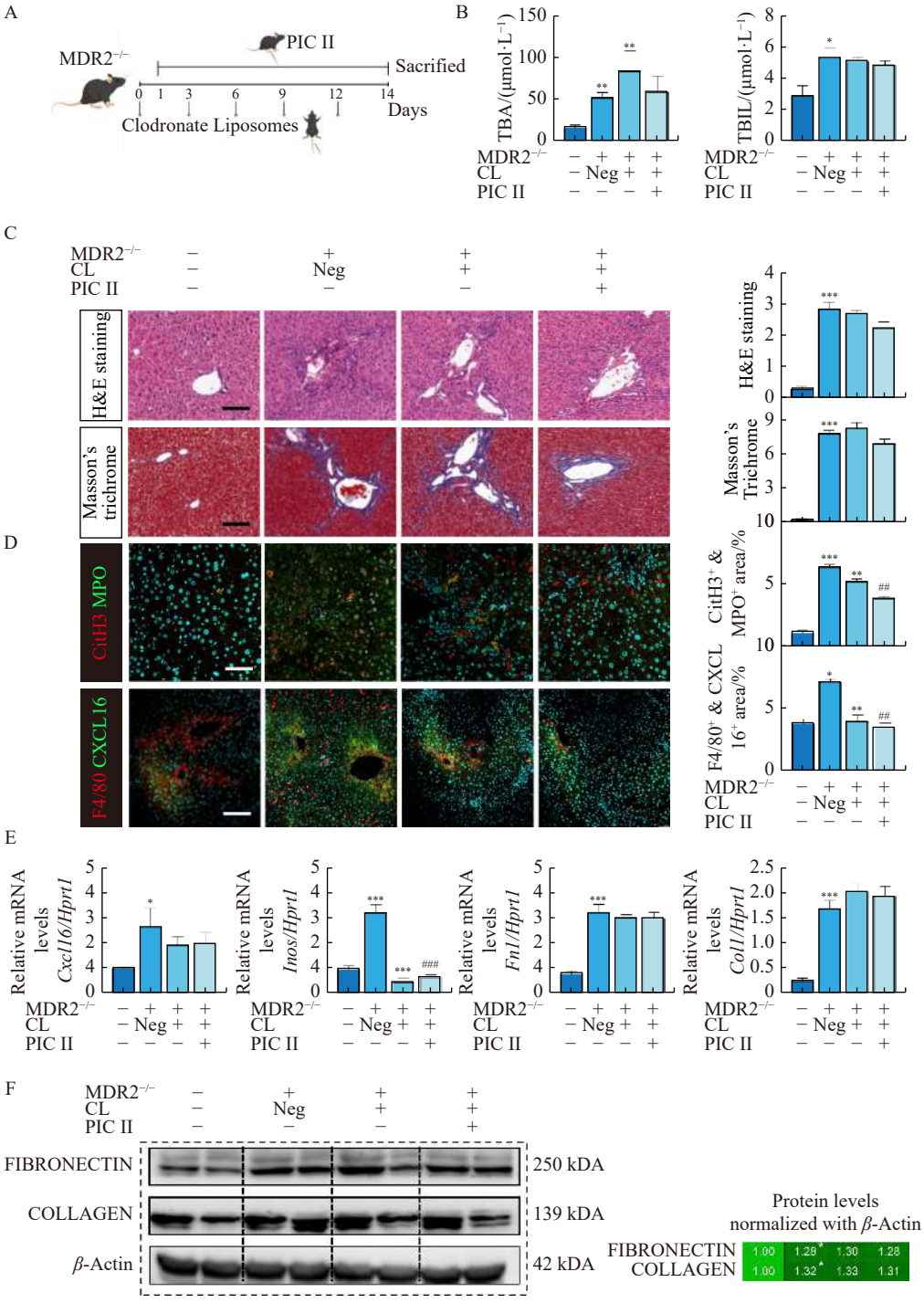

Fig. 8 Depletion of macrophages partially neutralizes the anti-fibrotic effect of PIC II. (A) Flowchart of the animal experiment. (B) Serum levels of TBA and TBIL. (C) Representative images of H&E staining and Masson's trichome staining (Scale bar = 20 μm). (D) Representative images of immunofluorescence staining for NET formation (CitH3 and MPO) and the co-staining of F4/80 and CXCL16 in the liver (Scale bar = 20 μm). (E) Relative mRNA levels of *Cxcl16*, *Inos*, *Fn1*, and *Col1a1* were measured by qPCR and further normalized with *Hprt1*. (F) The protein levels of FIBRONECTIN and COLLAGEN were measured by Western blotting analysis and normalized by *β*-Actin in the liver. Quantifications were performed using Image J. Data are presented as the mean ± SEM (n = 6). Statistical significance: $^{*}P < 0.05$, $^{**}P < 0.01$, $^{***}P < 0.001$ *vs* the WT group; $^{\#\#}P < 0.01$, $^{\#\#\#}P < 0.001$ *vs* the Mdr2$^{-/-}$ group.

downregulated both in the Mdr2$^{-/-}$ + CL group and the Mdr2$^{-/-}$ + CL + PIC II group. Additionally, we observed the following changes in other immune cell markers: the phagosome marker *Rab7a* remained unchanged, the cytotoxic marker of NK cells *Il4* was slightly decreased, and the neutrophil marker *Ly6g* was upregulated in the Mdr2$^{-/-}$ + CL group but downregulated in the Mdr2$^{-/-}$ + CL + PIC II group, indicating that PIC II might have an inhibitory effect on neutrophils in the liver fibrotic process. Interestingly, along with the changes in immune cell markers, the expression of fibrotic genes such as *Fn1*, *Col1a1* and *Acta2* remained high, and PIC II could not decrease their expression after macrophage depletion in Mdr2$^{-/-}$ mice (Fig. 8E and Fig. S9B). Similarly, the protein levels of FIBRONECTIN and COLLAGEN Fig. 8F showed the same trend in these groups, and the Jak1/Tyk2-STAT1 proteins in liver tissues also showed inconspicuous changes after macrophage depletion, even with PIC II treatment (Fig. S9C). These results suggest that macrophage depletion at least partially neutralized the hepatoprotective effects induced by PIC II in Mdr2$^{-/-}$ mice.

Discussion

Liver fibrosis is a global epidemic characterized by the activation of myofibroblasts, which secrete ECM proteins, and chronic, interminable inflammation initiated and exacerbated by macrophages, dendritic cells, NK cells, and neutrophils. In the complex hepatic immune network, macrophages generally initiate adaptive immune inflammatory responses and stimulate paracellular cells to release various cytokines, profoundly affecting the activation, senescence, or apoptosis of HSCs [27, 28]. In this study, we explored the anti-fibrotic effect of PIC II on liver fibrosis in Mdr2$^{-/-}$ mice and found that PIC II might inhibit the activation of HSCs by affecting various immune cells. Specifically, an increase in M1-polarized macrophages was observed in the livers of Mdr2$^{-/-}$ mice treated with PIC II, accompanied by highly expressed CXCL16 and significantly decreased fibrotic markers (Figs. 1 and 2). Although PIC II exerted a slight inhibitory effect on aHSCs, it significantly promoted the function of M1-polarized macrophages without inducing inflammation and facilitated the release of CXCL16 into the extracellular environment (Fig. 3). We also noticed that M1-polarized macrophages were accompanied by the gathering of NK cells in Mdr2$^{-/-}$ mice, which were potentially recruited by CXCL16 released from PIC II-treated M1 macrophages through CXCR6 expressed on the NK cell surface (Fig. 4). Furthermore, under the stimulation of PIC II, the IFN-γ secreted by NK cells might activate and phosphorylate the JAK1/TYK2 , promoting the nuclear translocation of STAT1 and eventually inducing cell death in activated HSCs (Fig. 6). Additionally, PIC II exhibited an inhibitory effect on neutrophils by blocking NET formation and possibly inducing neutrophil senescence, ultimately preventing the severe inflammatory cascade that activates HSCs in the fibrotic environment (Fig. 7). Notably, the depletion of macrophages largely counteracted the protective effects of PIC II (Fig. 8).

As the central immune cells in the liver fibrosis process, macrophages play a crucial role in both regulating the deposition and breakdown of ECM. Emerging studies have shown that distinct macrophage subsets exert bidirectional roles and contribute to different pathological outcomes of liver fibrosis [29, 30]. M1 macrophages are increasingly being targeted for cryotherapy due to their anti-liver fibrosis effects, which include recruiting endogenous macrophages and NK cells to inhibit HSC proliferation [25]. Furthermore, we speculated that the growing CXCL16 secretion by macrophages might intervene in the liver fibrosis process. CXCL16 levels were increased in the sequencing data of Mdr2$^{-/-}$ mouse liver and PIC II-treated groups, and CXCL16 has been previously reported to inhibit liver fibrosis [31, 32]. In this study, PIC II markedly increased M1-polarized macrophages and promoted the secretion of CXCL16 in the fibrotic environment, although macrophages exerted a limited direct inhibitory effect on aHSCs (Figs. 2 and 3). We hypothesized that macrophage-derived CXCL16 enhances the ability of NK cells to kill aHSCs through the indirect CXCL16-CXCR6 pathway, as previously reported [32-34]. Consistently, we observed enhanced cell-killing ability of NK cells on aHSCs under the influence of CM-M, with increased recruitment of NK cells. Thus, we propose that CXCL16-positive M1 macrophages may recruit NK cells and inhibit liver fibrosis in Mdr2$^{-/-}$ mice through CXCR6 expressed on the surface of NK cells in concert with CXCL16. This mechanism underscores the potential of targeting the CXCL16-CXCR6 axis to enhance the anti-fibrotic effects of macrophages and NK cells, providing a novel therapeutic approach for treating liver fibrosis.

The increase in both the quantity and activity of NK cells has been acknowledged to have a beneficial effect in alleviating the progression of liver fibrosis [35]. NK cells can directly promote HSC apoptosis and ultimately hinder fibrogenesis through the upregulation of GZMB and PERFORIN [36, 37]. Additionally, we hypothesized that NK cells interfere with the activation pathway of HSCs *via* IFN-γ related signaling. Typically, IFN-γ binds to its receptors IFNGR1 and IFNGR2 [38, 39], promoting the phosphorylation of JAKs, TYK2 and STAT1. The activation of STAT1 promotes apoptotic signaling in aHSCs, thereby limiting the development of liver fibrosis. Recently, Alberto and colleagues demonstrated that rilpivirine could ameliorate liver fibrosis by selectively activating STAT1-dependent apoptosis in HSCs and STAT3-dependent regeneration in hepatocytes to promote liver reconstruction [26]. Similarly, our study reveals that NK cells treated with CM from PIC II-treated M1-polarized macrophages induced apoptosis in aHSCs, accompanied by the activation of the IFN-γ-JAK1/TAK2-STAT1 pathway, rather than directly killing HSCs by secreting cytotoxic GZMB and PERFORIN in Mdr2$^{-/-}$ mice (Figs. 5 and 6). Moreover, FXR activation is generally inhibited in Mdr2$^{-/-}$ mice, and PIC II alleviates α-naphthylisothiocyanate-induced cholestatic liver injury by activating the FXR pathway to modulate the bile acid homeo-

stasis [13, 40]. The promoter of FXR has been shown to be regulated by STAT1 as a transcription activator [41]. Although the mutual relationship between FXR and STAT1 in NK-HSC communication has not yet been verified in this process, the potential mechanism by which PIC II mediates STAT1 through regulating FXR warrants further investigation. These results provide a perspective to understand the interaction between NK cells recruited by macrophages and HSCs in liver fibrosis. Specifically, our findings suggest that PIC II enhances the anti-fibrotic effects of NK cells by promoting the IFN-γ-JAK1/TYK2-STAT1 signaling pathway, offering a potential therapeutic approach for treating liver fibrosis through the modulation of immune cell interactions and signaling pathways.

Interestingly, we also observed a trend of neutrophil gene set activation and NET formation in the livers of Mdr2$^{-/-}$ mice. Previously, NETosis has been more commonly observed in conditions such as Non-alcoholic steatohepatitis (NASH), liver cirrhosis/necrosis, and hepatocellular carcinoma [42, 43]. However, the MPO-citH3 index and the NET formation results in liver tissue from our study support the hypothesis that NET formation also occurs in the fibrotic and inflammatory environment of Mdr2$^{-/-}$ mouse livers. We found a correlation between NET formation and HSC activation in Mdr2$^{-/-}$ mice, and PIC II administration not only inhibited NETosis but also reduced collagen formation during the fibrotic process. Interestingly, CXCR4, often treated as a marker of aged neutrophils, is a receptor that allows for the clearance of neutrophils in the bone marrow [44]. Our results showed that Cxcr4 was upregulated in neutrophils recruited during fibrosis and downregulated following PIC II administration, suggesting the possibility of neutrophil senescence and providing a potential mechanism by which PIC II exerts its effects in the liver fibrotic environment. However, the role and pattern of NETs in the activation of HSCs and the relationships between neutrophils, M1 macrophages, and NK cells in this study remain uncertain and warrant further exploration.

It is noteworthy that macrophages, as candidates for the treatment of liver fibrosis, exhibit different polarization states and a wide range of plasticity. Selective macrophage depletion has been shown to reduce BDL-induced fibrotic liver injury, accompanied by inhibition of the long non-coding RNA H19 (lncRNA H19). Overexpression of H19, however, can counteract the effects of macrophage depletion in liver fibrosis [45]. On the other hand, an important fact that cannot be ignored is that CL cannot selectively deplete specific subtypes of macrophages in the liver. Consequently, another study reported that macrophage depletion *via* CL had no therapeutic effect on bile duct expansion in the livers of Anks6$^{-/-}$ mice [46]. Ideally, to test our hypothesis, we would selectively knock out CXCL16 in liver macrophages. However, this approach is limited by two factors: 1) Perfect nanoparticle vectors that specifically target CXCL16 in liver macrophages may not yet be available; 2) The strong chemotactic signals produced by M1 macrophage-derived CXCLs are unavoidable in the complex *in vivo* environment. Therefore, in our study, we chose to deplete macrophages using CL and found that this method effectively influenced the release of CXCL16 and partially blocked the anti-fibrotic effects of PIC II on the livers of Mdr2$^{-/-}$ mice (Fig. 8). Thus, the use of CL depletion alone may lead to complex and contradictory outcomes due to the diverse functions of hepatic macrophages. Whether this method can be used effectively for the treatment of liver fibrosis remains to be determined.

Conclusion

Collectively, our study highlights the importance of M1 macrophage-centered interactions among immune cells in the fibrotic livers of Mdr2$^{-/-}$ mice. We demonstrated that PIC II, by modulating these immune interactions, shows potential as a candidate for halting the progression of liver fibrosis. Through enhancing the function of M1 macrophages, promoting NK cell activity, and inhibiting neutrophil-mediated inflammation and NET formation, PIC II effectively mitigates the fibrotic process.

Supporting Information

Supporting information of this paper can be requested by sending E-mail to the corresponding author.

References

[1] Parola M, Pinzani M. Liver fibrosis: pathophysiology, pathogenetic targets and clinical issues [J]. *Mol Aspects Med*, 2019, **65**: 37-55.

[2] Hammerich L, Tacke F. Hepatic inflammatory responses in liver fibrosis [J]. *Nat Rev Gastroenterol Hepatol*, 2023, **20**(10): 633-646.

[3] Shah RA, Kowdley KV. Current and potential treatments for primary biliary cholangitis [J]. *Lancet Gastroenterol Hepatol*, 2020, **5**(3): 306-315.

[4] Liu Y, Chen K, Li F, *et al*. Probiotic *Lactobacillus rhamnosus* GG prevents liver fibrosis through inhibiting hepatic bile acid synthesis and enhancing bile acid excretion in mice [J]. *Hepatology*, 2020, **71**(6): 2050-2066.

[5] Zhang J, Lyu Z, Li B, *et al*. P4HA2 induces hepatic ductular reaction and biliary fibrosis in chronic cholestatic liver diseases [J]. *Hepatology*, 2023, **78**(1): 10-25.

[6] Liu R, Li X, Zhu W, *et al*. Cholangiocyte-derived exosomal long noncoding RNA H19 promotes hepatic stellate cell activation and cholestatic liver fibrosis [J]. *Hepatology*, 2019, **70**(4): 1317-1335.

[7] Yoshida S, Ikenaga N, Liu SB, *et al*. Extrahepatic platelet-derived growth factor-β, delivered by platelets, promotes activation of hepatic stellate cells and biliary fibrosis in mice [J]. *Gastroenterology*, 2014, **147**(6): 1378-1392.

[8] Guicciardi ME, Trussoni CE, Krishnan A, *et al*. Macrophages contribute to the pathogenesis of sclerosing cholangitis in mice [J]. *J Hepatol*, 2018, **69**(3): 676-686.

[9] Shi T, Malik A, Yang VH, *et al*. Farnesoid X receptor antagonizes macrophage-dependent licensing of effector T lymphocytes and progression of sclerosing cholangitis [J]. *Sci Transl Med*, 2022, **14**(675): eabi4354.

[10] Greenman R, Segal-Salto M, Barashi N, *et al*. CCL24 regulates biliary inflammation and fibrosis in primary sclerosing

cholangitis [J]. *JCI Insight*, 2023, **8**(12): e162270.
[11] Ravichandran G, Neumann K, Berkhout LK, *et al*. Interferon-γ-dependent immune responses contribute to the pathogenesis of sclerosing cholangitis in mice [J]. *J Hepatol*, 2019, **71**(4): 773-782.
[12] Taylor AE, Carey AN, Kudira R, *et al*. Interleukin 2 promotes hepatic regulatory T cell responses and protects from biliary fibrosis in murine sclerosing cholangitis [J]. *Hepatology*, 2018, **68**(5): 1905-1921.
[13] Li T, Xu L, Zheng R, *et al*. Picroside II protects against cholestatic liver injury possibly through activation of farnesoid X receptor [J]. *Phytomedicine*, 2020, **68**: 153153.
[14] Ma S, Wang X, Lai F, *et al*. The beneficial pharmacological effects and potential mechanisms of picroside II: evidence of its benefits from *in vitro* and *in vivo* [J]. *Biomed Pharmacother*, 2020, **130**: 110421.
[15] Duan S, Li X, Fan G, *et al*. Targeting bile acid signaling for the treatment of liver diseases: from bench to bed [J]. *Biomed Pharmacother*, 2022, **152**: 113154.
[16] Huang Y, Zhou M, Li C, *et al*. Picroside II protects against sepsis *via* suppressing inflammation in mice [J]. *Am J Transl Res*, 2016, **8**(12): 5519-5531.
[17] Wang Y, Hong Y, Zhang C, *et al*. Picroside II attenuates hyperhomocysteinemia-induced endothelial injury by reducing inflammation, oxidative stress and cell apoptosis [J]. *J Cell Mol Med*, 2019, **23**(1): 464-475.
[18] Li Y J, Liu RP, Ding MN, *et al*. Tetramethylpyrazine prevents liver fibrotic injury in mice by targeting hepatocyte-derived and mitochondrial DNA-enriched extracellular vesicles [J]. *Acta Pharmacol Sin*, 2022, **43**(8): 2026-2041.
[19] Sliz A, Locker KCS, Lampe K, *et al*. Gab3 is required for IL-2- and IL-15-induced NK cell expansion and limits trophoblast invasion during pregnancy [J]. *Sci Immunol*, 2019, **4**(38): eaav3866.
[20] Fehniger TA, Carson WE, Mrózek E, *et al*. Stem cell factor enhances interleukin-2-mediated expansion of murine natural killer cells *in vivo* [J]. *Blood*, 1997, **90**(9): 3647-3653.
[21] Melhem A, Muhanna N, Bishara A, *et al*. Anti-fibrotic activity of NK cells in experimental liver injury through killing of activated HSC [J]. *J Hepatol*, 2006, **45**(1): 60-71.
[22] Casini A, Ceni E, Salzano R, *et al*. Neutrophil-derived superoxide anion induces lipid peroxidation and stimulates collagen synthesis in human hepatic stellate cells: role of nitric oxide [J]. *Hepatology*, 1997, **25**(2): 361-367.
[23] Zhou Z, Xu MJ, Cai Y, *et al*. Neutrophil-hepatic stellate cell interactions promote fibrosis in experimental steatohepatitis [J]. *Cell Mol Gastroenterol Hepatol*, 2018, **5**(3): 399-413.
[24] Cheng D, Chai J, Wang H, *et al*. Hepatic macrophages: key players in the development and progression of liver fibrosis [J]. *Liver Int*, 2021, **41**(10): 2279-2294.
[25] Ma PF, Gao CC, Yi J, *et al*. Cytotherapy with M1-polarized macrophages ameliorates liver fibrosis by modulating immune microenvironment in mice [J]. *J Hepatol*, 2017, **67**(4): 770-779.
[26] Martí-Rodrigo A, Alegre F, Moragrega ÁB, *et al*. Rilpivirine attenuates liver fibrosis through selective STAT1-mediated apoptosis in hepatic stellate cells [J]. *Gut*, 2020, **69**(5): 920-932.
[27] Li YW, Lu YR, Nian MZ, *et al*. Therapeutic potential and mechanism of Chinese herbal medicines in treating fibrotic liver disease [J]. *Chin J Nat Med*, 2023, **21**(9): 643-657.
[28] Kisseleva T, Brenner D. Molecular and cellular mechanisms of liver fibrosis and its regression [J]. *Nat Rev Gastroenterol Hepatol*, 2021, **18**(3): 151-166.
[29] Tacke F. Targeting hepatic macrophages to treat liver diseases [J]. *J Hepatol*, 2017, **66**(6): 1300-1312.
[30] Rao J, Wang H, Ni M, *et al*. FSTL1 promotes liver fibrosis by reprogramming macrophage function through modulating the intracellular function of PKM2 [J]. *Gut*, 2022, **71**(12): 2539-2550.
[31] Korbecki J, Bajdak-Rusinek K, Kupnicka P, *et al*. The role of CXCL16 in the pathogenesis of cancer and other diseases [J]. *Int J Mol Sci*, 2021, **22**(7): 3490.
[32] Mossanen JC, Kohlhepp M, Wehr A, *et al*. CXCR6 inhibits hepatocarcinogenesis by promoting natural killer T- and $CD4^{(+)}$ T-cell-dependent control of senescence [J]. *Gastroenterology*, 2019, **156**(6): 1877-1889.e4.
[33] Xu HB, Gong YP, Cheng J, *et al*. CXCL16 participates in pathogenesis of immunological liver injury by regulating T lymphocyte infiltration in liver tissue [J]. *World J Gastroenterol*, 2005, **11**(32): 4979-4985.
[34] Liepelt A, Wehr A, Kohlhepp M, *et al*. CXCR6 protects from inflammation and fibrosis in NEMO(LPC-KO) mice [J]. *Biochim Biophys Acta Mol Basis Dis*, 2019, **1865**(2): 391-402.
[35] Tsuchida T, Friedman SL. Mechanisms of hepatic stellate cell activation [J]. *Nat Rev Gastroenterol Hepatol*, 2017, **14**(7): 397-411.
[36] Choi WM, Ryu T, Lee JH, *et al*. Metabotropic glutamate receptor 5 in natural killer cells attenuates liver fibrosis by exerting cytotoxicity to activated stellate cells [J]. *Hepatology*, 2021, **74**(4): 2170-2185.
[37] Chigbu DI, Loonawat R, Sehgal M, *et al*. Hepatitis C virus infection: host-virus interaction and mechanisms of viral persistence [J]. *Cells*, 2019, **8**(4): E376.
[38] Wen J, Zhou Y, Wang J, *et al*. Interactions between Th1 cells and Tregs affect regulation of hepatic fibrosis in biliary atresia through the IFN-γ/STAT1 pathway [J]. *Cell Death Differ*, 2017, **24**(6): 997-1006.
[39] Guo M, Wang Z, Dai J, *et al*. Glycyrrhizic acid alleviates liver fibrosis *in vitro* and *in vivo via* activating CUGBP1-mediated IFN-γ/STAT1/Smad7 pathway [J]. *Phytomedicine*, 2022, **112**: 154587.
[40] Li T, Zheng R, Xu L, *et al*. Picroside II alleviates liver injury induced by alpha-naphthylisothiocyanate through AMPK-FXR pathway [J]. *Toxicol Appl Pharmacol*, 2020, **408**: 115248.
[41] Li M, Zhang X, Lu Y, *et al*. The nuclear translocation of transketolase inhibits the farnesoid receptor expression by promoting the binding of HDAC3 to FXR promoter in hepatocellular carcinoma cell lines [J]. *Cell Death Dis*, 2020, **11**(1): 31.
[42] Wu J, Zhang C, He T, *et al*. Polyunsaturated fatty acids drive neutrophil extracellular trap formation in nonalcoholic steatohepatitis [J]. *Eur J Pharmacol*, 2023, **945**: 175618.
[43] Scozzi D, Gelman AE. Avoid being trapped by your liver: ischemia-reperfusion injury in liver transplant triggers S1P-mediated NETosis [J]. *J Clin Invest*, 2023, **133**(3): e167012.
[44] Zhang D, Chen G, Manwani D, *et al*. Neutrophil ageing is regulated by the microbiome [J]. *Nature*, 2015, **525**(7570): 528-532.
[45] Tian X, Wang Y, Lu Y, *et al*. Conditional depletion of macrophages ameliorates cholestatic liver injury and fibrosis *via* lncRNA-H19 [J]. *Cell Death Dis*, 2021, **12**(7): 646.
[46] Airik M, McCourt B, Ozturk TT, *et al*. Mitigation of portal fibrosis and cholestatic liver disease in ANKS6-deficient livers by macrophage depletion [J]. *FASEB J*, 2022, **36**(2): e22157.

Cite this article as: JIA Kexin, MA Zhi, ZHANG Yinhao, *et al*. Picroside II promotes HSC apoptosis and inhibits the cholestatic liver fibrosis in $Mdr2^{-/-}$ mice by polarizing M1 macrophages and balancing immune responses [J]. *Chin J Nat Med*, 2024, **22**(7): 582-598.